# Terahertz spectroscopy study of the confining potential for methane in the endofullerene $CH_4@C_{60}$

Tanzeeha Jafari,¹ Anna Shugai,¹ Urmas Nagel,¹ Elizabeth S. Marsden,² Sally Bloodworth,² Gabriela Hoffman,² George R. Bacanu,² Mark C. Walkey,² Malcolm H. Levitt,² Richard J. Whitby,² and Toomas Rõõm¹

<sup>1)</sup>National Institute of Chemical Physics and Biophysics, Tallinn, 12618, Estonia

<sup>2)</sup>School of Chemistry and Chemical Engineering, University of Southampton, Southampton, SO171BJ,

(\*Electronic mail: toomas.room@kbfi.ee)

(Dated: 31 July 2025)

We used terahertz spectroscopy to study the non-covalent interaction between  $CH_4$  and the confining fullerene cage in endofullerene  $CH_4@C_{60}$ . The temperature dependence of the THz absorption spectra of powdered  $CH_4@C_{60}$  was measured between 5 and 300 K. At temperatures below 50 K, the THz spectrum of  $CH_4$  shows a single line centered at 214 cm<sup>-1</sup>, which broadens and shifts to higher energy as the temperature increases. These effects are explained by the anharmonicity of the  $CH_4$ – $C_{60}$  interaction potential function. The model involves the center-of-mass motion of  $CH_4$  in a spherically symmetric potential well. Line intensities are modeled by invoking an electric dipole moment induced by the translational displacement of  $CH_4$  from the center of the cage  $C_{60}$ . The potential function and the dipole moment parameters were derived from the temperature dependence of the THz absorption spectra and compared with the parameters of previously studied endofullerenes. The quantum chemistry calculations reproduce the  $CH_4$  translation motion frequency and the potential function remarkably well.

### I. INTRODUCTION

After the discovery of fullerene C<sub>60</sub> by Kroto et al.<sup>1</sup> in 1985, this highly symmetric molecule gained immediate attention due to its potential to encapsulate atoms and molecules in its hollow cavity. Soon the same group of scientists reported the encapsulation of lanthanum atom by laser ablation method to form La@C<sub>60</sub><sup>2</sup>, known as endofullerene and denoted as  $A@C_{60}$ . Since then, the field of studies of endofullerenes has shown significant growth. The advent of the "molecular surgery" method<sup>3</sup> has allowed for the synthesis of a variety of endohedral fullerenes in relatively large amount<sup>4</sup>. These includes noble gas atoms<sup>5–8</sup> and molecular species such as  $H_2@C_{60}^{9}$ ,  $H_2@C_{70}^{10}$ ,  $HF@C_{60}^{11}$ ,  $H_2O@C_{60}^{12}$ ,  $CH_4@C_{60}^{13}$ , and  $CH_2O@C_{60}^{14}$ . One salient feature of the confinement is the quantization of the center-of-mass translational degrees of freedom of the guest species. This phenomenon, thanks to "molecular surgery" is accessible to various spectroscopic techniques and has been studied in detail for endofullerenes hosting noble gas atoms and small molecules by terahertz (THz) and infrared spectroscopy 10,14–24 and inelastic neutron scattering spectroscopy 18,20,22,25–30

The confining potential energy function of atoms and small molecules inside the  $C_{60}$  molecular cage is the result of nonbonding interactions between the guest and  $C_{60}$ . This function has been a frequent target of theoretical calculations  $^{31-46}$ . The noble gas atoms are spherically symmetric and only have translational degrees of freedom, which makes them a relatively simple system for quantum chemistry calculations. The calculation of more complicated endohedral species in which the guest is a polar molecule, such as  $H_2O$  and  $HF@C_{60}$ , has been widely regarded as a challenge. Endofullerenes like  $CH_4@C_{60}$ , in which the molecule fits tightly inside the cage, also presents computational difficulties. The quantum chemistry calculation often requires a careful selection of compu-

tational techniques and the basis set to precisely determine the weak non-bonding interactions. Therefore, experimental findings which guide the selection of computational model and the basis set, are highly valuable. Over the years, reliable potential energy functions have been determined for  $H_2 @ C_{60}^{15-17,29}$  and noble gas atoms<sup>21,22</sup>. The translational excitation frequencies from the ground to the first excited state have been determined for  $HF@C_{60}^{18}$ ,  $H_2O@C_{60}^{19}$ , and  $CH_2O@C_{60}^{14}$ . However, to the best of our knowledge, no potential energy function nor translational excitation frequency has so far been determined experimentally for a larger molecule such as  $CH_4@C_{60}$ .  $CH_4@C_{60}$  has been the subject of several theoretical studies, including the prediction of terhertz and infrared spectra<sup>47-49</sup>.

Here we report a THz study of translational dynamics of CH<sub>4</sub> in the molecular cavity of  $C_{60}$ . To determine the anharmonicity of the confining potential, we studied the temperature dependence of the THz absorption spectra. CH<sub>4</sub> is classified as a spherical top molecule, for which the translation-rotation coupling is expected to be negligible compared to less symmetric molecules such as  $H_2@C_{60}^{16}$ ,  $HF@C_{60}^{18}$ ,  $H_2O@C_{60}^{19}$  and  $CH_2O@C_{60}^{14}$ . Hence, the translation motion of  $CH_4@C_{60}$  can be treated independently of its rotations, and the Hamiltonian model is similar to that of a confined noble gas atom<sup>20</sup>.

### **II. MATERIALS AND METHODS**

### A. Sample preparation

CH<sub>4</sub>@C<sub>60</sub> sample was prepared using the multiroute "molecular surgery" method<sup>13</sup>. The procedure involves a series of controlled chemical reactions to create a hole in the fullerene molecule cage, then incorporating the guest species

through the hole, and finally closing the hole with another series of chemical reactions while keeping the guest inside the fullerene

Following the synthesis, the  $CH_4@C_{60}$  sample was subjected to high-performance liquid chromatography (HPLC) to remove the traces of empty  $C_{60}$ . Eventually,  $CH_4@C_{60}$  was obtained with filling factor  $f_0 = 100.0 \pm 0.3\%$ . The sample was sublimed under a vacuum before THz measurements.

### B. Measurement technique

The CH<sub>4</sub>@C<sub>60</sub> powdered sample (12.7 mg) was put into the 3 mm brass frame and pressed into a d = 1.1 mm thick pellet.

To achieve cryogenic temperatures a cold-finger continuous flow cryostat was used, equipped with a sample cell. The brass frame containing the pressed pellet was placed into the vacuum-tight sample cell with two thin polypropylene windows. The sample cell was filled with 100 mbar of He gas at room temperature to facilitate good thermal contact between the cold finger and the pellet. The cryostat was inserted into the sample compartment of the interferometer. The transmission spectra of  $CH_4@C_{60}$  were measured up to  $300~cm^{-1}$  using a FTIR Bruker Vertex 80v spectrometer equipped with SiC (globar) radiation source, a  $6\mu m$  thick Mylar beamsplitter, and a 4~K bolometer detector. The spectral resolution was  $0.3~cm^{-1}$ , which was less than the line width of  $CH_4@C_{60}$  absorption lines.

To record the transmission spectra, the cold finger was moved up and down relative to the beam, allowing the light to pass through the sample or a 3 mm reference hole attached to the cold finger. The transmission spectra,  $T(\omega)$ , were measured as the ratio of the intensity of light transmitted through sample,  $I_s(\omega)$  at frequency  $\omega$ , to the intensity transmitted by the reference hole,  $I_r(\omega)$ ,  $T(\omega) = I_s(\omega)/I_r(\omega)$ . The absorption spectra  $\alpha(\omega)$  were calculated from the transmission spectra,  $\alpha(\omega) = -d^{-1} \ln \left[ T(\omega) R(\omega)^{-1} \right]$ , where d is the sample thickness.  $R(\omega)$  is the amount of radiation lost in reflections from the surfaces of the pellet and sample chamber windows. Since R is featureless in the spectral range of CH<sub>4</sub> absorption lines it was subtracted as a background absorption without affecting the CH<sub>4</sub> absorption line intensities and shape.

## C. Confined $\mathrm{CH}_4$ translational motion: Anharmonic spherical oscillator model

To describe the quantized translational motion of  $CH_4$  trapped inside the  $C_{60}$  we use the spherical anharmonic oscillator model. The detailed formulation of the model has been discussed in Ref.20 and Ref.21. Here, we summarize the key features. We treat  $C_{60}$  as a rigid body with a fixed center of mass. Within this approximation, we ignore the effects of  $C_{60}$  rotations and librations on the motion of the confined  $CH_4$ . We also ignore the coupling of  $CH_4$  to the vibrations of  $C_{60}$  and to the crystal lattice modes. We assume the confining potential stays constant over the 5 to 300 K temperature range.

Fullerene has icosahedral symmetry, but for simplicity, we approximate it with spherical symmetry. This approximation excludes any angular dependence and as a result, the potential function of  $\mathrm{CH_4}$  depends only on the radial displacement r from the  $\mathrm{C_{60}}$  center of mass.

The Hamiltonian  $\hat{H}$  for CH<sub>4</sub> in the spherically symmetric potential is

$$\hat{H} = \frac{\hat{p}^2}{2m} + V_2 r^2 + V_4 r^4,\tag{1}$$

where  $V_4r^4$  is the anharmonic correction. The first two terms are the kinetic and potential energy of the harmonic oscillator with the energy eigenvalues

$$E_n = \hbar \omega_0 \left( n + \frac{3}{2} \right), \tag{2}$$

where the frequency of the harmonic spherical oscillator is  $\omega_0 = \sqrt{2V_2/m}$  and m is the mass of CH<sub>4</sub>. The eigenstates of the harmonic spherical oscillator are well known<sup>21,50</sup>. They are characterized by translational quantum number,  $n \in \{1,2,3...\}$  and angular momentum quantum number  $\ell$ , where  $\ell \in \{2,4,6...\}$  for even n and  $\ell \in \{1,3,5...\}$  for odd n. The anharmonic spherically symmetric Hamiltonian of CH<sub>4</sub> is solved by diagonalizing Eq. (1) numerically using a finite basis set of harmonic spherical oscillator eigenstates, using all the states up to and including  $n_{max} = 18$ . Since the potential is spherically symmetric, there is no mixing of eigenstates with different  $\ell$  and the energy levels are  $(2\ell+1)$ -fold degenerate.

The translational motion of  $CH_4$  is decoupled from electromagnetic radiation since the molecule is neutral. We assume that the electric field of THz radiation couples to the dipole moment induced by the displacement of  $CH_4$  from the center of the  $C_{60}$  cage,  $\mathbf{r}=(r,\phi,\theta)$ , given in spherical coordinates. A similar analysis was used to treat the THz spectrum of  $He@C_{60}^{21}$ . The dipole moment operator, as discussed in Ref.21, is expressed as a function of spherical harmonic of rank one,

$$d_{1q} = \sqrt{\frac{4\pi}{3}} A_{1q} r Y_{1q}(\theta, \phi), \tag{3}$$

where  $A_{1q}$  is the real-valued dipole amplitude coefficient and  $q \in \{-1,0,+1\}$ . For spherical symmetry,  $A_{1q}$  does not depend on q, so  $A_{1q} \equiv A_1$ . In case of CH<sub>4</sub>@C<sub>60</sub>, we found that it was not necessary to include higher order odd powers of r in the expansion Eq. (3). The selection rules for the electric dipole transition of harmonic oscillator are  $\Delta \ell = \pm 1$  and  $\Delta n = \pm 1^{21}$ .

The fitting parameters  $\kappa = \{V_2, V_4, A_1\}$  are determined by minimizing the difference-squared between the baseline-corrected experimental spectrum and the spectrum calculated with the fitting parameters. At each step the Hamiltonian was diagonalized numerically and the dipole moment matrix transformed into the Hamiltonian eigenbasis. The line intensities were calculated by taking into account the thermal populations of the energy levels as described in Ref. 21. The linewidth of the CH<sub>4</sub>@C<sub>60</sub> experimental spectra changes with temperature. Up to 80 K the full width at half maximum

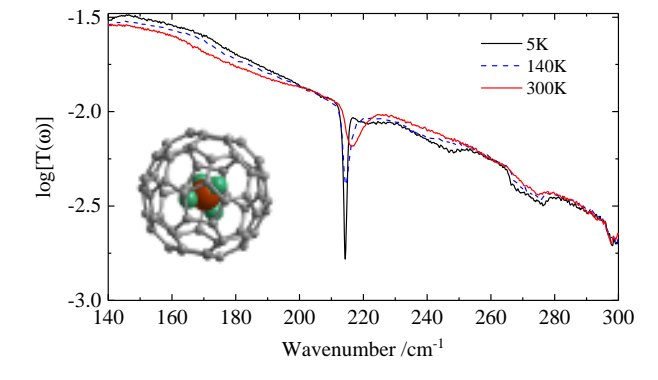


FIG. 1. Temperature dependence of THz transmission spectra of CH<sub>4</sub>@C<sub>60</sub> at 5 K (black solid line), 140 K (dashed blue line) and 300 K (red solid line). Plotted is the  $\log_{10}[T(\omega)]$  where  $T(\omega) = I_s(\omega)/I_r(\omega)$  and  $I_s$  and  $I_r$  are the intensities transmitted through the sample and through the reference hole, respectively.

was determined from the experimental spectra. Above  $80\,\mathrm{K}$  it was not possible to resolve individual lines and therefore the linewidth was assumed to be equal to  $2~\mathrm{cm}^{-1}$  and independent of temperature. The confidence limits of the fit parameters were calculated with the method described in Ref.19.

### D. Quantum chemistry calculations

The structure of  $CH_4@C_{60}$  was minimised with Gaussian 09 revision  $D1.01^{51}$  using Density Functional Theory (DFT) with pure  $PB86^{52,53}$  functional, and the harmonic frequencies calculated for the translational modes. The basis set was  $cc\text{-pVDZ}^{54}$  with a superfine (175,974 points for H, 250,974 points for C) integration grid. Tight criteria were used for convergence.

### III. RESULTS AND DISCUSSIONS

The temperature dependence of THz transmission spectra of  $CH_4@C_{60}$  is shown in Fig. 1. At the lowest temperature of 5 K, the THz spectrum displays one prominent absorption line at 214 cm<sup>-1</sup>. As the temperature increases the absorption line broadens and shifts to higher frequency. The peak is exclusive to  $CH_4@C_{60}$  because such a peak is present in the THz spectra of neither  $C_{60}$  nor  $A@C_{60}$ . The peak does not belong to the vibrational mode of free  $CH_4$  because all of the vibrational modes frequencies are above  $1200~\text{cm}^{-1}$ . Also, it is not the rotational transition of  $CH_4@C_{60}$  because the rotational constant is small,  $B = 5.2~\text{cm}^{-155}$ , which correspond to  $10.4~\text{cm}^{-1}$  energy difference between the ground and the first excited rotational state.

A more detailed temperature dependence of the absorption spectra with the baseline subtracted is shown in Fig. 2. We attribute the  $214~\rm cm^{-1}$  peak in the THz absorption spectrum to the quantized center-of-mass translational motion of CH<sub>4</sub> inside C<sub>60</sub>. The peak broadening and the shifts of its maximum to higher frequency is due to the increased population of

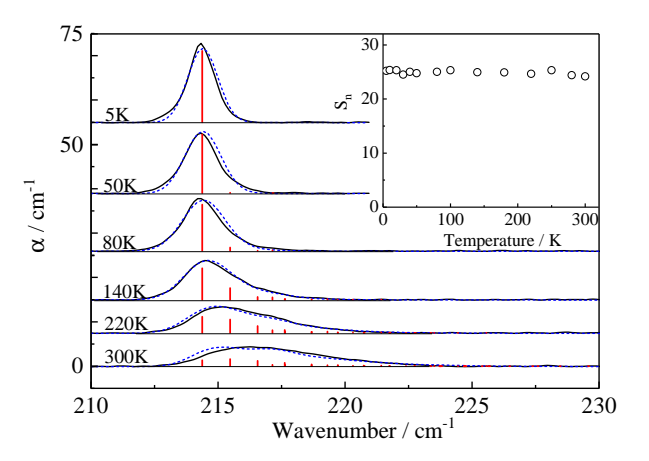


FIG. 2. Temperature dependence of THz absorption spectra of  $CH_4@C_{60}$ . Experimental spectra (black) and the calculated spectra (blue dashed) using best fit parameters given in Table I. Calculated spectra are plotted using Gaussian line shape and T-dependent line width, see text. Sticks represent positions of individual lines from the model fit with stick height proportional to the line area. The inset shows the integrated line area across measured temperatures.

excited translational states at higher temperature; transitions starting from excited translational states have an increased energy due to the anharmonicity of the potential function. The inset to Fig. 2 shows that the total line area does not change with temperature. This confirms that all electric-dipole-active transitions of CH<sub>4</sub> translational motion are contained within the same peak.

To validate our experimental findings, we fitted the experimental spectra with the spherical anharmonic oscillator model, Sec. II C. This model only includes calculations of the frequencies and intensities, and does not take into account line width effects. To obtain the experimental line widths the low temperature spectra were fitted with a single Gaussian line from where the temperature-dependent line widths followed:  $(T/K, FWHM / cm^{-1})$ : (5, 1.4), (10, 1.4), (20, 1.52), (30, 1.55), (40, 1.6), (50, 1.68), (60, 1.77), (80, 1.93). Since the individual lines could not be resolved in the experimental spectra above 80 K, the line width was assumed constant, 2 cm<sup>-1</sup>, in the spectra measured at 100, 140, 180, 220, 250 280 and 300 K. When fitting the spectra with the anharmonic oscillator model these line widths were used to calculate the model spectra. The model spectra, calculated using the best fit potential and dipole moment parameters listed in Table I are plotted in Fig. 2 for selected temperatures. In Table II we list the energy levels up to n = 5 calculated with the best fit potential parameters.

The anharmonic spherical oscillator parameters that give the best fit to the experimental THz spectra are given in Table I. The anharmonic  $V_4$  term is positive, which means that the distance between the energy levels increases with increasing energy. This behaviour is found for all  $A@C_{60}$  species, as shown in Table I. The effect of positive  $V_4$  term is visible in Fig. 2: the additional absorption lines in the high temperature

TABLE I. The best fit polynomial coefficients and their confidence limits for the spherically symmetric potential function  $V(r) = V_2 r^2 + V_4 r^4 + V_6 r^6$  and induced dipole function  $d = (4\pi/3)^{1/2} (A_1 r + A_3 r^3) Y_{10}(\theta, \phi)$  of  $A@C_{60}$ .  $d_{01} = \langle 1 | d | 0 \rangle$  is the expectation value of the dipole moment between the ground state and the first excited state.  $\omega_{01}$  is the peak frequency of the absorption line at 5 K in the measured THz spectrum which corresponds to the energy separation of the ground state and the first excited state.  $v_{anh} = (\omega_{01} - \omega_0)/\omega_{01}$  is the fractional contribution of the anharmonic potential to  $\omega_{01}$  where  $\omega_0 = (2\pi c)^{-1} \sqrt{2V_2/m}$  is the frequency of the harmonic oscillator, Eq. (2), in wavenumber units and c is the speed of light in vacuum.  $R_W$  is the van der Waals radius of A. The data for atoms is from Ref. 21 and Ref. 22.

Parameter

4He

20Ne

40Ar

CH<sub>4</sub>

Parameter	<sup>4</sup> He	<sup>20</sup> Ne	<sup>40</sup> Ar	<sup>84</sup> Kr	CH <sub>4</sub>
$V_2 / \rm{Jm}^{-2}$	$0.39 \pm 0.006$	$1.58 \pm 0.04$	$9.56 \pm 0.03$	$17.81 \pm 0.12$	$21.10 \pm 0.04$
$V_4/\mathrm{J}\mathrm{m}^{-4}/10^{20}$	$(0.60 \pm 0.01)$	$(2.28 \pm 0.22)$	$(8.19 \pm 0.16)$	$(13.2 \pm 1.60)$	$(11.6 \pm 0.56)$
$V_6/\mathrm{Jm^{-6}/10^{39}}$	$(3.94 \pm 0.09)$	0	0	0	0
$A_1/C/10^{-21}$	$(0.68 \pm 0.04)$	$(1.84 \pm 0.13)$	$(3.31 \pm 0.01)$	$(3.30 \pm 0.21)$	$(2.73 \pm 0.03)$
$A_3 / C m^{-2}$	$0.04 \pm 0.01$	0	0	0	0
$d_{01}/\mathrm{Debye}$	0.017	0.019	0.020	0.014	0.017
$\omega_{01}$ / cm <sup>-1</sup>	81.4	56.6	91.8	85.4	214.1
$v_{\rm anh}$	0.29	0.085	0.018	0.007	0.014
$R_{ m W}$ / pm	140 <sup>56</sup>	154 <sup>56</sup>	188 <sup>56</sup>	$202^{56}$	$206^{57}$

spectra appear on the higher frequency side of the low temperature absorption line. However, the transitions from thermally excited energy levels merge because of the small energy separation of individual lines relative to the line width, resulting in a single broad unresolved line. Similar behaviour is observed for endofullerenes containing the noble gas atoms Ne, Ar, and  $Kr^{22}$ . This contrasts to the case of He@C\_{60}, which shows a comb of well-resolved peaks as the excited levels become thermally populated at high temperatures  $^{20}$ .

TABLE II. Translational energy levels of CH<sub>4</sub>@C<sub>60</sub> obtained from the fits of THz absorption spectra.  $|\xi|^2$  is the amplitude-squared of the dominant component of the eigenstate with the quantum numbers  $(n, \ell)$ . The zero point energy, 319.47 cm<sup>-1</sup>, has been subtracted.

E/ cm <sup>-1</sup>	n	$\ell$	$ \xi ^2$
0	0	0	1
214.4	1	1	1
429.9	2	2	1
431.5	2	0	0.999
646.4	3	3	0.999
649.2	3	1	0.998
864.0	4	4	0.998
867.8	4	2	0.997
869.5	4	0	0.996
1082.7	5	5	0.998
1087.6	5	3	0.995
1090.2	5	1	0.994
	1		

Anharmonicity in the confining potential induces mixing between the harmonic oscillator eigenstates. Hence, a good indicator of the degree of anharmonicity is the largest coefficient of a harmonic oscillator state in each eigenstate of the anharmonic oscillator. This coefficient is equal to 1 for a harmonic oscillator but takes a smaller value for an anharmonic oscillator. Table II lists the computed coefficients for the anharmonic oscillator eigenstates used to match the experimental THz spectrum of  $CH_4@C_{60}$ , as shown in Figure 2. In case of  $CH_4$ ,  $|\xi|^2$  falls off slowly with increasing n indicating the weak anharmonicity of the potential function. For example,

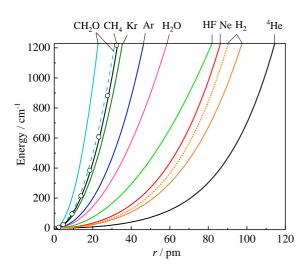


FIG. 3. The experimentally determined potential energy curve V(r) of several endohedral complexes of  $C_{60}$ . The potential energy curves of  $^4$ He,  $^{20}$ Ne,  $^{40}$ Ar,  $^{84}$ Kr and CH<sub>4</sub> are calculated with parameters from Table I. The open symbols are the result of quantum chemistry calculation for CH<sub>4</sub>@C<sub>60</sub>, see Section II D. The potential curves of H<sub>2</sub> are calculated from best fit parameters given in Ref.16, where the H<sub>2</sub> molecule axis is parallel to the displacement  ${\bf r}$  (dotted orange) and perpendicular to it (solid orange). The degree of anharmonicity of HF, H<sub>2</sub>O and CH<sub>2</sub>O@C<sub>60</sub> is not known experimentally. Here the potential curve is plotted in harmonic approximation where  $V_2 = m\omega_0^2/2$  and  $\omega_0 (2\pi c)^{-1}$  is the observed translational frequency in wavenumber units:  $78.6 \text{ cm}^{-1}$  for HF@C<sub>60</sub><sup>18</sup>,  $110 \text{ cm}^{-1}$  for H<sub>2</sub>O@C<sub>60</sub><sup>19</sup> and 166.8 (dashed) and 231.1 cm<sup>-1</sup> (solid) for CH<sub>2</sub>O@C<sub>60</sub><sup>14</sup>; c is the speed of light in vacuum.

the  $|\xi|^2$  in the state which is predominantly  $(n,\ell)=(3,3)$ , is 0.69 in  $^4\text{He}@\text{C}_{60}{}^{21}$  while it is 0.999 in CH<sub>4</sub>@C<sub>60</sub>.

Just like other  $A@C_{60}$  in Table I,  $CH_4$  is neutral and lacks permanent dipole moment. The guest molecule gains the dipole moment through its interaction with the inner surface of  $C_{60}$  when it moves away from the cage center. The induced

This is the author's peer reviewed, accepted manuscript. However, the online version of record will be different from this version once it has been copyedited and typeset

PLEASE CITE THIS ARTICLE AS DOI: 10.1063/5.0289052

dipole moment,  $\langle 0|d|1\rangle$ , of CH<sub>4</sub> and atoms for the transition from the ground (n=0) to the first excited state (n=1) is listed in Table I. It can be seen that the induced dipole moments are about 100 times smaller than the permanent dipole moment of free H<sub>2</sub>O (1.85D), for example.

Previous DFT studies on CH<sub>4</sub>@C<sub>60</sub> using the Becke-Perdew BP86 exchange-correlation functional 52,53 gave the translational mode frequencies of 209, 217, and  $220 \text{ cm}^{-147}$ . Although the mean (215.3 cm<sup>-1</sup>) is in exceptionally good agreement with the experimental value  $(214 \text{ cm}^{-1})$  the wide spread of values does not reflect the high symmetry of the CH<sub>4</sub>@C<sub>60</sub> system. Repeating the calculation using a large integration grid gave translational mode frequencies of 207.3, 207.5 and 208.1 cm<sup>-1</sup>. Although the mean  $(207.6 \text{ cm}^{-1})$  is further from that observed the narrow spread of three calculated mode frequencies is an improvement. A potential energy curve for the 207.5 cm<sup>-1</sup> translational mode was constructed using single point energy calculations on structures generated along the mode using GaussView and is shown in Fig. 3. The calculated potential provides an overall good description of the confining potential of the encapsulated CH<sub>4</sub> molecule.

In Fig. 3, we also compare the experimentally derived potential energy function curves of several endohedral complexes of C<sub>60</sub>. The comparison of CH<sub>4</sub>@C<sub>60</sub> and Noble gas atoms shows that there is a correlation with the van der Waals radius (listed in Table I): the potential steepens with the increase of the van der Waals radius. This conforms to the intuitive picture that large species fit more snugly into the C<sub>60</sub> cavity and have less room to "rattle around". The comparison to other four molecules is not so straightforward. Firstly, H<sub>2</sub>, HF, H<sub>2</sub>O and CH<sub>2</sub>O are asymmetric; this asymmetry, manifested as translation-rotation coupling in the Hamiltonian <sup>15,36</sup>, is demonstrated for H<sub>2</sub> where two potential curves are shown, for the H<sub>2</sub> molecule axis parallel and perpendicular to the displacement vector r; although the anisotropic experimental potential curves have not been derived for CH<sub>2</sub>O@C<sub>60</sub>. the translation-rotation coupling must be strong in comparison to H<sub>2</sub> as the two well-separated lines are seen at 166.8 and 231.1 cm<sup>-1</sup> in the CH<sub>2</sub>O@C<sub>60</sub> THz absorption spectrum<sup>14</sup>. Secondly, there is no experimental data about the anharmonicity for  $H_2O@C_{60}$ ,  $HF@C_{60}$  and  $CH_2O@C_{60}$ .

To summarize, the translational mode of  $CH_4$  was observed at  $214~\rm cm^{-1}$  at 5 K in the molecular cavity of  $C_{60}$ . The potential energy curve, including the anharmonic correction, was determined from the temperature dependence of the THz absorption spectra which shift to higher energy and broaden as the temperature increases. The THz spectra are well described by a spherical anharmonic oscillator for the  $CH_4$  center-of-mass motion despite the internal vibrational and rotational degrees of freedom of  $CH_4$ . The experimentally determined potential function is in good agreement with quantum chemistry calculations. The lighter mass of  $CH_4$  combined with the steep confining potential sets the  $CH_4@C_{60}$  mode frequency to be higher than that of  $C_{60}$  endofullerenes containing noble gas atoms in  $C_{60}$ .

### **AUTHOR CONTRIBUTIONS**

E.S.M., M.C.W., G.H., S.B., and R.J.W. carried out synthesis and purification of endofullerenes. T.J., A.S., U.N., and T.R. performed the THz experiments and processed the THz data. T.J., and T.R. derived the potential parameters by fitting the THz spectra. R.J.W. performed the quantum chemistry calculation. T.J. wrote an initial draft of the paper. T.R. developed the concept of the paper. All authors reviewed and developed the manuscript.

### **ACKNOWLEDGMENTS**

This research was supported by the Estonian Ministry of Education, personal research funding PRG736, and the European Regional Development Fund project TK134, and by EPSRC grants EP/T004320/1, EP/P009980/1 and EP/Y010515/1 of UK. RJW acknowledges the use of the IRIDIS High Performance Computing Facility at the University of Southampton.

### DATA AVAILABILITY STATEMENT

The data that support the findings of this study are available from the corresponding author upon reasonable request.

- <sup>1</sup>H. Kroto, J. Heath, S. O'Brian, R. F. Curl, and R. E. Smalley, "C<sub>60</sub>: Buck-minsterfullerene," Nature **318**, 162–163 (1985).
- <sup>2</sup>J. R. Heath, S. C. O'Brien, Q. Zhang, Y. Liu, R. F. Curl, F. K. Tittel, and R. E. Smalley, "Lanthanum complexes of spheroidal carbon shells," J. Am. Chem. Soc. **107**, 7779–7780 (1985), http://pubs.acs.org/doi/pdf/10.1021/ja00311a102.
- $^3$ K. Komatsu, M. Murata, and Y. Murata, "Encapsulation of Molecular Hydrogen in Fullerene  $C_{60}$  by Organic synthesis," Science **307**, 238–240 (2005).
- <sup>4</sup>S. Bloodworth and R. J. Whitby, "Synthesis of endohedral fullerenes by molecular surgery," Commun. Chem. **5** (2022), 10.1038/s42004-022-00738-9
- <sup>5</sup>Y. Morinaka, F. Tanabe, M. Murata, Y. Murata, and K. Komatsu, "Rational synthesis, enrichment, and <sup>13</sup>C NMR spectra of endohedral C<sub>60</sub> and C<sub>70</sub> encapsulating a helium atom," Chem. Commun. **46**, 4532–4534 (2010).
- <sup>6</sup>S. Bloodworth, G. Hoffman, M. C. Walkey, G. R. Bacanu, J. M. Herniman, M. H. Levitt, and R. J. Whitby, "Synthesis of Ar@C<sub>60</sub> using molecular surgery," Chem. Commun. 56, 10521–10524 (2020).
- <sup>7</sup>G. Hoffman, M. C. Walkey, J. Gräsvik, G. R. Bacanu, S. Alom, S. Bloodworth, M. E. Light, M. H. Levitt, and R. J. Whitby, "A Solid-State Intramolecular Wittig Reaction Enables Efficient Synthesis of Endofullerenes Including Ne@C<sub>60</sub>, <sup>3</sup>He@C<sub>60</sub>, and HD@C<sub>60</sub>," Angew. Chem. Int. Ed. **60**, 8960–8966 (2021).
- <sup>8</sup>G. Hoffman, G. R. Bacanu, E. S. Marsden, M. C. Walkey, M. Sabba, S. Bloodworth, G. J. Tizzard, M. H. Levitt, and R. J. Whitby, "Synthesis and <sup>83</sup>Kr NMR spectroscopy of Kr@C<sub>60</sub>," Chem. Commun. **58**, 11284–11287 (2022).
- <sup>9</sup>M. Murata, Y. Murata, and K. Komatsu, "Synthesis and properties of endohedral C<sub>60</sub> encapsulating molecular hydrogen," J. Am. Chem. Soc. **128**, 8024–8033 (2006).
- <sup>10</sup>T. Rõõm, L. Peedu, M. Ge, D. Hüvonen, U. Nagel, S. Ye, M. Xu, Z. Bačić, S. Mamone, M. H. Levitt, M. Carravetta, J. Chen, X. Lei, N. J. Turro, Y. Murata, and K. Komatsu, "Infrared spectroscopy of small-molecule end-ofullerenes." Phil. Trans. R. Soc. A 371, 20110631 (2013).
- <sup>11</sup> A. Krachmalnicoff, M. H. Levitt, and R. J. Whitby, "An optimised scalable synthesis of H<sub>2</sub>O@C<sub>60</sub> and a new synthesis of H<sub>2</sub>@C<sub>60</sub>," Chem. Commun. 50, 13037–13040 (2014).

- <sup>12</sup>M. Murata, Y. Murata, and K. Komatsu, "Organic synthesis of endohedral fullerenes encapsulating helium, dihydrogen, and water," in *Organic Nanomaterials* (John Wiley & Sons, Ltd, 2013) Chap. 11, pp. 225–239, https://onlinelibrary.wiley.com/doi/pdf/10.1002/9781118354377.ch11.
- <sup>13</sup>S. Bloodworth, G. Sitinova, S. Alom, S. Vidal, G. R. Bacanu, S. J. Elliott, M. E. Light, J. M. Herniman, G. J. Langley, M. H. Levitt, and R. J. Whitby, "First synthesis and characterization of CH<sub>4</sub>@C<sub>60</sub>," Angew. Chem. Int. Ed. 58, 5038–5043 (2019).
- <sup>14</sup>V. K. Vyas, G. R. Bacanu, M. Soundararajan, E. S. Marsden, T. Jafari, A. Shugai, M. E. Light, U. Nagel, T. Rõõm, M. H. Levitt, and R. J. Whitby, "Squeezing formaldehyde into C<sub>60</sub> fullerene," Nat Commun 15 (2024), 10.1038/s41467-024-46886-5.
- <sup>15</sup>S. Mamone, M. Ge, D. Hüvonen, U. Nagel, A. Danquigny, F. Cuda, M. C. Grossel, Y. Murata, K. Komatsu, M. H. Levitt, T. Rõõm, and M. Carravetta, "Rotor in a cage: Infrared spectroscopy of an endohedral hydrogenfullerene complex," J. Chem. Phys. 130, 081103 (2009).
- <sup>16</sup>M. Ge, U. Nagel, D. Hüvonen, T. Rõõm, S. Mamone, M. H. Levitt, M. Carravetta, Y. Murata, K. Komatsu, J. Y.-C. Chen, and N. J. Turro, "Interaction potential and infrared absorption of endohedral H<sub>2</sub> in C<sub>60</sub>." J. Chem. Phys. 134, 054507 (2011).
- <sup>17</sup>M. Ge, U. Nagel, D. Hüvonen, T. Rõõm, S. Mamone, M. H. Levitt, M. Carravetta, Y. Murata, K. Komatsu, X. Lei, and N. J. Turro, "Infrared spectroscopy of endohedral HD and D<sub>2</sub> in C<sub>60</sub>," J. Chem. Phys. **135**, 114511 (2011).
- <sup>18</sup>A. Krachmalnicoff, R. Bounds, S. Mamone, S. Alom, M. Concistrè, B. Meier, K. Kouříl, M. E. Light, M. R. Johnson, S. Rols, A. J. Horsewill, A. Shugai, U. Nagel, T. Rõõm, M. Carravetta, M. H. Levitt, and R. J. Whitby, "The dipolar endofullerene HF@C<sub>60</sub>," Nat. Chem. 8, 953–957 (2016)
- <sup>19</sup>A. Shugai, U. Nagel, Y. Murata, Y. Li, S. Mamone, A. Krachmalnicoff, S. Alom, R. J. Whitby, M. H. Levitt, and T. Rõõm, "Infrared spectroscopy of an endohedral water in fullerene," J. Chem. Phys. **154**, 124311 (2021).
- <sup>20</sup>G. R. Bacanu, T. Jafari, M. Aouane, J. Rantaharju, M. Walkey, G. Hoffman, A. Shugai, U. Nagel, M. Jiménez-Ruiz, A. J. Horsewill, S. Rols, T. Rõõm, R. J. Whitby, and M. H. Levitt, "Experimental determination of the interaction potential between a helium atom and the interior surface of a C<sub>60</sub> fullerene molecule," J. Chem. Phys. **155**, 144302 (2021), https://doi.org/10.1063/5.0066817.
- <sup>21</sup>T. Jafari, G. R. Bacanu, A. Shugai, U. Nagel, M. Walkey, G. Hoffman, M. H. Levitt, R. J. Whitby, and T. Rõõm, "Terahertz spectroscopy of the helium endofullerene He@C<sub>60</sub>," Phys. Chem. Chem. Phys. **24**, 9943–9952 (2022).
- <sup>22</sup>T. Jafari, A. Shugai, U. Nagel, G. R. Bacanu, M. Aouane, M. Jiménez-Ruiz, S. Rols, S. Bloodworth, M. Walkey, G. Hoffman, R. J. Whitby, M. H. Levitt, and T. Rõõm, "Ne, Ar, and Kr oscillators in the molecular cavity of fullerene C<sub>60</sub>," J. Chem. Phys. 158 (2023), 10.1063/5.0152628, https://pubs.aip.org/aip/jcp/article-pdf/doi/10.1063/5.0152628/18005120/234305\_1\_5.0152628.pdf.
- <sup>23</sup>T. Putaud, J.-C. Chartrand, Y. Kalugina, X. Michaut, P.-N. Roy, and P. Ayotte, "A simple confined rotor model to describe the ro-translational dynamics of water endofullerenes and to assign the ro-vibrational spectra of solid H<sub>2</sub>O@C<sub>60</sub>," J. Chem. Phys. 162 (2025), 10.1063/5.0253540.
- <sup>24</sup>J.-C. Chartrand, T. Putaud, G. Bélanger, M. Bertin, J.-H. Fillion, P. Léveillé, X. Michaut, and P. Ayotte, "Signatures of rotation—translation couplings, symmetry-breaking, and intermolecular interactions in the rovibrational spectra of solid H<sub>2</sub>O@C<sub>60</sub>," J. Chem. Phys. **162** (2025), 10.1063/5.0253539.
- <sup>25</sup>A. J. Horsewill, S. Rols, M. R. Johnson, Y. Murata, M. Murata, K. Komatsu, M. Carravetta, S. Mamone, M. H. Levitt, J. Y.-C. Chen, J. A. Johnson, X. Lei, and N. J. Turro, "Inelastic neutron scattering of a quantum translator-rotator encapsulated in a closed fullerene cage: Isotope effects and translation-rotation coupling in H<sub>2</sub>@C<sub>60</sub> and HD@C<sub>60</sub>," Phys. Rev. B 82, 081410 (2010).
- <sup>26</sup> A. J. Horsewill, K. S. Panesar, S. Rols, J. Ollivier, M. R. Johnson, M. Carravetta, S. Mamone, M. H. Levitt, Y. Murata, K. Komatsu, J. Y.-C. Chen, J. A. Johnson, X. Lei, and N. J. Turro, "Inelastic neutron scattering investigations of the quantum molecular dynamics of a H<sub>2</sub> molecule entrapped inside a fullerene cage," Phys. Rev. B 85, 205440 (2012).
- <sup>27</sup>A. J. Horsewill, K. Goh, S. Rols, J. Ollivier, M. R. Johnson, M. H. Levitt, M. Carravetta, S. Mamone, Y. Murata, J. Y.-C. Chen, J. A. Johnson, X. Lei,

- and N. J. Turro, "Quantum rotation and translation of hydrogen molecules encapsulated inside C<sub>60</sub>: temperature dependence of inelastic neutron scattering spectra," Phil. Trans. R. Soc. A **371**, 20110627 (2013).
- <sup>28</sup>K. S. K. Goh, M. Jimenez-Ruiz, M. R. Johnson, S. Rols, J. Ollivier, M. S. Denning, S. Mamone, M. H. Levitt, X. Lei, Y. Li, N. J. Turro, Y. Murata, and A. J. Horsewill, "Symmetry-breaking in the endofullerene H<sub>2</sub>O@C<sub>60</sub> revealed in the quantum dynamics of ortho and para-water: a neutron scattering investigation," Phys. Chem. Chem. Phys. 16, 21330–21339 (2014).
- <sup>29</sup>S. Mamone, M. Jiménez-Ruiz, M. R. Johnson, S. Rols, and A. J. Horsewill, "Experimental, theoretical and computational investigation of the inelastic neutron scattering spectrum of a homonuclear diatomic molecule in a nearly spherical trap: H<sub>2</sub>@C<sub>60</sub>," Phys. Chem. Chem. Phys. 18, 29369–29380 (2016).
- <sup>30</sup>M. Aouane, J. Armstrong, M. Walkey, G. Hoffman, G. R. Bacanu, R. J. Whitby, M. H. Levitt, and S. Rols, "A combined inelastic neutron scattering and simulation study of the <sup>3</sup>He@C<sub>60</sub> endofullerene," Phys. Chem. Chem. Phys. 25, 20295–20301 (2023).
- <sup>31</sup>C. Williams, M. Whitehead, and L. Pang, "Interaction and dynamics of endohedral gas molecules in C<sub>60</sub> isomers and C<sub>70</sub>," J. Phys. Chem. **97**, 11652–11656 (1993).
- <sup>32</sup>L. Pang and F. Brisse, "Endohedral energies and translation of fullerenenoble gas clusters G@Cn (g = helium, neon, argon, krypton and xenon: n = 60 and 70)," J. Phys. Chem. 97, 8562–8563 (1993).
- <sup>33</sup>H. A. Jiménez-Vázquez and R. J. Cross, "Equilibrium constants for noblegas fullerene compounds," J. Chem. Phys. 104, 5589–5593 (1996).
- <sup>34</sup>E. H. T. Olthof, A. van der Avoird, and P. E. S. Wormer, "Vibration and rotation of CO in C<sub>60</sub> and predicted infrared spectrum," J. Chem. Phys. **104**, 832–847 (1996).
- <sup>35</sup>R. J. Cross, "Does H<sub>2</sub> rotate freely inside fullerenes?" J. Phys. Chem. A 105, 6943 (2001).
- <sup>36</sup>M. Xu, F. Sebastianelli, Z. Bačić, R. Lawler, and N. J. Turro, "Quantum dynamics of coupled translational and rotational motions of H<sub>2</sub> inside C<sub>60</sub>," J. Chem. Phys. **128**, 011101 (2008).
- $^{37}M.$  Xu, F. Sebastianelli, Z. Bačić, R. Lawler, and N. J. Turro, "H<sub>2</sub> , HD, and D<sub>2</sub> inside C<sub>60</sub>: Coupled translation-rotation eigenstates of the endohedral molecules from quantum five-dimensional calculations," J. Chem. Phys. **129**, 064313 (2008).
- <sup>38</sup>P. M. Felker and Z. Bačić, "Communication: Quantum six-dimensional calculations of the coupled translation-rotation eigenstates of H<sub>2</sub>O@C<sub>60</sub>," J. Chem. Phys. **144**, 201101 (2016), http://dx.doi.org/10.1063/1.4953180.
- <sup>39</sup>P. M. Felker and Z. Bačić, "Translation-rotation states of H<sub>2</sub> in C<sub>60</sub>: New insights from a perturbation-theory treatment," J. Chem. Phys. **145** (2016), 10.1063/1.4961650.
- <sup>40</sup>P-N. R. Kalugina Y. N., "Potential energy and dipole moment surfaces for hf@c60: Prediction of spectral and electric response properties," The journal of chemical physics **147**, 244303 (2017).
- <sup>41</sup>Z. Bačić, V. Vlček, D. Neuhauser, and P. M. Felker, "Effects of symmetry breaking on the translation-rotation eigenstates of H<sub>2</sub>, HF, and H<sub>2</sub>O inside the fullerene C<sub>60</sub>," Discuss. Faraday Soc. 212, 547–567 (2018).
- <sup>42</sup>E. Rashed and J. L. Dunn, "Interactions between a water molecule and C<sub>60</sub> in the endohedral fullerene H<sub>2</sub>O@C<sub>60</sub>," Phys. Chem. Chem. Phys. 21, 3347–3359 (2019).
- <sup>43</sup>M. Xu, P. M. Felker, S. Mamone, A. J. Horsewill, S. Rols, R. J. Whitby, and Z. Bačić, "The endofullerene HF@C<sub>60</sub>: Inelastic neutron scattering spectra from quantum simulations and experiment, validity of the selection rule, and symmetry breaking," J. Phys. Chem. Lett. 10, 5365–5371 (2019).
- <sup>44</sup>O. Carrillo-Bohórquez, Álvaro Valdés, and R. Prosmiti, "Encapsulation of a water molecule inside c<sub>60</sub> fullerene: The impact of confinement on quantum features," J. Chem. Theory Comput. 17, 5839–5848 (2021).
- <sup>45</sup>M. Xu, P. M. Felker, and Z. Bačić, "H<sub>2</sub>O@C<sub>60</sub> inside the fullerene C<sub>60</sub>: Inelastic neutron scattering spectrum from rigorous quantum calculations," J. Chem. Phys. **156**, 124101 (2022).
- <sup>46</sup>K. Panchagnula, D. Graf, F. E. A. Albertani, and A. J. W. Thom, "Translational eigenstates of He@C<sub>60</sub> from four-dimensional *ab initio* potential energy surfaces interpolated using gaussian process regression," J. Chem. Phys. 160, 104303 (2024).
- <sup>47</sup>A. Rehaman, L. Gagliardi, and P. Pyykkö, "Pocket and antipocket conformations for the CH<sub>4</sub>@C<sub>84</sub> endohedral fullerene," Int J Quantum Chem 107, 1162–1169 (2009).

This is the author's peer reviewed, accepted manuscript. However, the online version of record will be different from this version once it has been copyedited and typeset

PLEASE CITE THIS ARTICLE AS DOI: 10.1063/5.0289052

- <sup>48</sup>A. Jaworski and N. Hedin, "Local energy decomposition analysis and molecular properties of encapsulated methane in fullerene CH<sub>4</sub>@C<sub>60</sub>," Phys. Chem. Chem. Phys. (2021), 10.1039/d1cp02333k.
- <sup>49</sup>Z. Slanina, F. Uhlík, T. Akasaka, X. Lu, and L. Adamowicz, "A computational characterization of CH<sub>4</sub>@C<sub>60</sub>," Inorganics 12, 64.
- <sup>50</sup>S. Flügge, *Practical Quantum Mechanics*, Vol. 1 (Springer-Verlag (Berlin), 1971).
- 51 M. J. Frisch, G. W. Trucks, H. B. Schlegel, G. E. Scuseria, M. A. Robb, J. R. Cheeseman, G. Scalmani, V. Barone, B. Mennucci, G. A. Petersson, H. Nakatsuji, M. Caricato, X. Li, H. P. Hratchian, A. F. Izmaylov, J. Bloino, G. Zheng, J. L. Sonnenberg, M. Hada, M. Ehara, K. Toyota, R. Fukuda, J. Hasegawa, M. Ishida, T. Nakajima, Y. Honda, O. Kitao, H. Nakai, T. Vreven, J. A. Montgomery Jr., J. E. Peralta, F. Ogliaro, M. Bearpark, J. J. Heyd, E. Brothers, K. N. Kudin, V. N. Staroverov, T. Keith, R. Kobayashi, J. Normand, K. Raghavachari, A. Rendell, J. C. Burant, S. S. Iyengar, J. Tomasi, M. Cossi, N. Rega, J. M. Millam, M. Klene, J. E. Knox, J. B. Cross, V. Bakken, C. Adamo, J. Jaramillo, R. Gomperts, R. E. Stratmann, O. Yazyev, A. J. Austin, R. Cammi, C. Pomelli, J. W. Ochterski, R. L.
- Martin, K. Morokuma, V. G. Zakrzewski, G. A. Voth, P. Salvador, J. J. Dannenberg, S. Dapprich, A. D. Daniels, O. Farkas, J. B. Foresman, J. V. Ortiz, J. Cioslowski, and D. J. Fox, "Gaussian 09 Revision D.01," (2013), gaussian Inc., Wallingford CT.
- <sup>52</sup>J. P. Perdew, "Density-functional approximation for the correlation energy of the inhomogeneous electron gas," Phys. Rev. B 33, 8822–8824 (1986).
- <sup>53</sup>A. D. Becke, "Density-functional exchange-energy approximation with correct asymptotic behavior," Phys. Rev. A 38, 3098–3100 (1988).
- <sup>54</sup>T. H. Dunning, "Gaussian basis sets for use in correlated molecular calculations. i. the atoms boron through neon and hydrogen," J. Chem. Phys. 90, 1007–1023 (1989).
- <sup>55</sup>G. Herzberg, *Infrared and Raman Spectra of Polyatomic Molecules*, 1st ed., Molecular Spectra and Molecular Structure, Vol. II (D. Van Nostrand Company, Inc., 1954).
- <sup>56</sup> A. Bondi, "Van der Waals volumes and radii," J. Phys. Chem. **68**, 441–451 (1964).
- <sup>57</sup>C. W. Kammeyer and D. R. Whitman, "Quantum mechanical calculation of molecular radii. I. hydrides of elements of periodic groups IV through VII," J. Chem. Phys. **56**, 4419–4421 (1972).